© 2020. Published by The Company of Biologists Ltd | Journal of Cell Science (2020) 133, jcs249102. doi:10.1242/jcs.249102

RESEARCH ARTICLE

RAS-mediated suppression of PAR3 and its effects on SCC initiation and tissue architecture occur independently of hyperplasia

Ji Ling, Maria Sckaff, Manisha Tiwari, Yifang Chen, Jingting Li, Jackson Jones and George L. Sen*

ABSTRACT

Proper epithelial development and homeostasis depends on strict control of oriented cell division. Current evidence shows that this process is regulated by intrinsic polarity factors and external spatial cues. Owing to the lack of an appropriate model system that can recapitulate the architecture of the skin, deregulation of spindle orientation in human epithelial carcinoma has never been investigated. Here, using an inducible model of human squamous cell carcinoma (SCC), we demonstrate that RAS-dependent suppression of PAR3 (encoded by *PARD3*) accelerates epithelial disorganization during early tumorigenesis. Diminished PAR3 led to loss of E-cadherin-mediated cell adhesion, which in turn contributed to misoriented cell division. Pharmacological inhibition of the MAPK pathway downstream of RAS activation reversed the defects in PAR3 expression, E-cadherin-mediated cell adhesion and mitotic spindle orientation. Thus, temporal analysis of human neoplasia provides a powerful approach to study cellular and molecular transformations during early oncogenesis, which allowed identification of PAR3 as a critical regulator of tissue architecture during initial human SCC development.

KEY WORDS: Epidermis, Skin, Tumorigenesis, Polarity, Cell junction, Cell adhesion, Mitotic spindle orientation, Epithelial organization

INTRODUCTION

Non-melanoma skin cancer, which includes basal cell carcinoma (BCC) and squamous cell carcinoma (SCC), is the most prevalent cancer in the United States and was estimated to afflict 3.3 million individuals in 2012 (Rogers et al., 2015). Even though mortality rates associated with BCC and SCC are low, morbidity and hospitalization costs can significantly burden the patient and the healthcare system (Guy et al., 2015). Skin cancer occurs when molecular pathways that modulate tissue homeostasis are deregulated by mutagenic activation of oncogenes or inhibition of tumor suppressors, such as HRAS or P53, respectively (Hussein, 2005).

The skin undergoes constant self-renewal (Tadeu and Horsley, 2014). To maintain homeostasis, precise control over proliferation and growth arrest-associated terminal differentiation is essential. Oriented cell division plays a crucial role in the development and maintenance of complex tissues such as the skin (Bergstralh et al., 2017; Gillies and Cabernard, 2011). By controlling the angle of the mitotic spindle, the cell defines the position of daughter cells within the tissue, and thereby regulates tissue architecture and cell fate (Williams and Fuchs, 2013). The formation of the stratified layers of the skin is dependent on both symmetric and asymmetric cell division (Lechler and Fuchs, 2005; Poulson and Lechler, 2010). Epidermal basal cells can divide parallel to the basement membrane to generate two identical progenitor cells and facilitate tissue expansion. Alternatively, they can divide along the apico-basal axis, to produce one basal and one suprabasal cell, which then differentiate and contributes to the stratification of the skin. Two important factors can influence the orientation of cell division in the skin: (1) intrinsic cell polarity signals that localize the mitotic spindles along the apical-basal axis for asymmetric cell division, or laterally for symmetric cell division; and (2) extrinsic factors, such as cell adhesion factors, that guide spindle alignment relative to tissue geometry and/or mechanical tension (Box et al., 2019; di Pietro et al., 2016). Thus, disruptions in directional division, cell polarity and cell–cell junctions, and the resultant effects on proliferation and/or architecture can significantly contribute to tumor initiation and progression.

Accordingly, transcriptomic analysis of human tumor samples obtained from multiple cancer types (including SCC) in The Cancer Genome Atlas datasets has revealed differentially regulated gene expression of multiple proteins involved in these processes (e.g. cell cycle regulators, centromere, kinetochore and mitotic spindle assembly proteins, and cadherin and claudin family members) (Li et al., 2017). These types of studies provide understanding of dysregulated cellular processes in established tumors, and can help to uncover potential targetable pathways in disease mitigation. However, functional analysis to determine whether these observed genetic changes are correlative or causative for disease has been hampered by the lack of rapid model systems that mimic human tissue (Khavari, 2006).

We believe that temporal analysis of tumor initiation and progression is key to understanding the initial molecular and cellular changes during tumorigenesis that dictate the aggressiveness of cancer growth. As nearly 90% of human cancers originate from the epithelium (McCaffrey and Macara, 2011), our study aims to understand the regulation of key molecular targets involved in cellular and tissue organization in human skin carcinoma. To closely model human SCC, we engineered three-dimensional (3D) organotypic skin that combines normal human dermis and primary human keratinocytes, which we then transplanted onto an immunodeficient mouse (Lazarov et al., 2002; Reuter et al., 2009). The resulting xenograft phenotypically resembles human skin, with proper epithelial stratification, an intact basement membrane and

Department of Dermatology, Department of Cellular and Molecular Medicine, UCSD Stem Cell Program, University of California, San Diego, La Jolla, CA 92093-0869, USA.

*Author for correspondence (gsen@health.ucsd.edu)

J.J., 0000-0002-6447-5166; G.L.S., 0000-0003-1279-8550

Handling Editor: Andrew Ewald
Received 18 May 2020; Accepted 27 October 2020

Journal of Cell Science (2020) 133, jcs249102. doi:10.1242/jcs.249102

extracellular matrix. Tumorigenesis in this setting is achieved by co-expression of CDK4 and conditionally active oncogenic HRAS. RAS mutations have been found in 30–40% of all cancers (Pickering et al., 2014), with HRAS being the most often mutated in SCCs (13–23%) (Dotto and Rustgi, 2016).

In this study, we found that, without HRAS activation, the human skin xenograft resembles human skin with normal distribution of cell division angles, polarity, and cell junction formation. Upon initiation of tumorigenesis, we observe a distinct temporal induction of hyper-proliferation, disordered cell division and disruption of claudin 1 (CLDN1)- and E-cadherin (ECAD, also known as CDH1)-mediated tight and adherens junction formation, respectively. Disruption in oriented cell division and cell–cell junctions were tightly correlated with decreased levels of cell polarity regulator partitioning defective 3 (PAR3; encoded by *PARD3*). Importantly, ectopic expression of PAR3 during tumor progression restored normal spindle orientation, as well as claudin 1- and E-cadherin-mediated junctions, but not tissue hyperplasia. Furthermore, we demonstrate that inhibition of a RAS downstream signaling pathway using U0126, a specific inhibitor of MEK1 and MEK2 (MEK1/2; also known as MAP2K1 and MAP2K2, respectively) (Favata et al., 1998), during tumorigenesis reversed PAR3 depletion and prevented loss of cell junctions and misorientation of mitotic spindles. Overall, we have identified PAR3 as a critical mediator of cell division orientation via regulation of intercellular adhesion in RAS-activated SCCs. Moreover, we demonstrate that RAS-dependent suppression of PAR3 protein accelerates epithelial disorganization in the early stages of SCC, which can be reversed by targeting MAPK signaling during tumor initiation.

RESULTS

Early human epidermal tumorigenesis is characterized by hyperplasia, and PAR3-dependent regulation of CLDN1- and ECAD-mediated tight and adherens junction formation

Studies in skin cancer patients over the past several decades have vastly increased our knowledge of established tumors in humans. However, much less is known about the changes that occur during initial tumor growth. To investigate the dysregulation of early cellular processes during tumorigenesis, we used an inducible model of human epidermal neoplasia. We co-expressed a tamoxifen (TMX)-inducible form of $HRAS^{G12V}$ (hereafter RAS) with CDK4 (denoted CDK4/RAS) in primary human keratinocytes grown on devitalized human dermis (Lazarov et al., 2002; Reuter et al., 2009). The resulting 3D human skin was then grafted onto immunodeficient mice (Fig. 1A). This regenerated skin results in a well-differentiated and stratified human epidermis, which remains phenotypically normal until TMX is introduced to drive oncogenic transformation. As expected, uninduced CDK4/RAS epidermis [vehicle (VEH); corn oil injections without TMX] displayed normal skin morphology (Fig. 1B). By contrast, TMX-dependent RAS activation resulted in altered tissue architecture and tumor progression (Fig. 1B).

TMX administration to CDK4/RAS xenografts resulted in progressive epidermal hyperplasia (Fig. 1B; Fig. S1A) and hyperproliferation as measured by Ki67 (also known as MKI67) staining (Fig. S1B,C). Gradual loss of differentiation marker keratin 10 (K10; also known as KRT10) (Fig. S1C) and degradation of the basement membrane (Fig. S1D) was also observed. These changes, which mimic the transformation of human epidermis to SCC, were further corroborated by transcriptional changes that indicate blockade of epidermal differentiation (*KRT2*), increased angiogenesis (*ITGB1*, *VEGFC*), increased matrix metalloproteinase expression that can disrupt basement membrane integrity (*MMP1*), and cancer signaling (*AREG*, *EREG*) (Fig. S1E). Notably, mRNA expression of known regulators of epithelial to mesenchymal transition (EMT) such as *SNAIL* (also known as *SNAI1*), *SLUG* (also known as *SNAI2*) and *TWIST2* were not significantly altered between normal and tumorigenic skin (Stemmler et al., 2019) (Fig. S1E). In addition, SNAIL and SLUG protein expression was not detectable in vehicle or RAS activated tissue for up to 20 days (Fig. S1F). This confirms that our observed period of RAS activation reflects the early stages of tumorigenesis and progression to metastasis has not yet occurred.

The absence of tissue organization is a hallmark of high-grade cancer (Hinck and Näthke, 2014). We assessed whether loss of epithelial organization was occurring in these early stages of tumor progression by quantifying the expression of CLDN1 (tight junction) and ECAD (adherens junction) during RAS activation. mRNA expression of *ECAD* and *CLDN1* did not differ between TMX- and VEH-treated grafts even at later time-points (Fig. S1E). Surprisingly, protein expression of CLDN1 and ECAD was visibly diminished at cell–cell junctions by days 15 and 20 of RAS activation (Fig. 1C,D,F), demonstrating the disruption of cell–cell adhesion mediated by these two proteins in the latter stages of tumor initiation. Interestingly, we noticed that protein expression of PAR3 was also markedly reduced at an even earlier time point (day 10) of TMX treatment (Fig. 1E,G). *PAR3* mRNA was not altered throughout the TMX treatment time course (Fig. S1E). To ensure that our results were not due to tamoxifen administration, normal human epidermis (without exogenous CDK4/RAS) grafted onto mice was treated with TMX for 20 days. The histology of the skin was normal and exhibited no signs of thickening or hyper-proliferation as compared to CDK4/RAS VEH-treated grafts (Fig. S1G,H). In addition, PAR3 and ECAD were expressed and properly localized to cell–cell junctions, suggesting that RAS activation rather than TMX administration caused the tumor-specific changes (Fig. S1I,J). Since decreased PAR3 protein expression precedes the loss of ECAD or CLDN1 from cell junctions in early tumorigenesis, we hypothesized that PAR3 may regulate CLDN1- and ECAD-mediated tight and adherens junction formation. To assess this, we constitutively expressed PAR3 in addition to RAS and CDK4 (denoted PAR3/CDK4/RAS) in regenerated human skin xenografts (Fig. 2A,B,D; Fig. S2A). In the absence of RAS activation (VEH day 20), PAR3 overexpression had no impact on normal keratinocyte tissue morphology, epithelial thickness, proliferation, expression of the epidermal differentiation gene *KRT2*, or ECAD or CLDN1 expression or localization (Fig. 2; Fig. S2B). Upon TMX treatment, ectopic PAR3 expression during tumorigenesis did not block hyper-proliferation, hyperplasia or downregulation of *KRT2* (Fig. 2B–F; Fig. S2A,B). However, PAR3 overexpression in TMX-induced tumorigenic CDK4/RAS xenografts did restore CLDN1 and ECAD expression at cell junctions (Fig. 2G,H; Fig. S2A), demonstrating the importance of PAR3 in regulating tight and adherens junctions during tumor initiation.

PAR3-dependent planar cell division is progressively lost during tumor initiation

PAR3 is a recognized regulator of apicobasal cell polarity (Lechler and Fuchs, 2005; Suzuki and Ohno, 2006; Xue et al., 2013; Zen et al., 2009). In embryonic mouse keratinocytes, mitotic spindle orientation and its resultant effect on daughter cell positioning are highly dependent on cell polarity (Williams et al., 2014). Given the importance of controlled symmetric versus asymmetric cell division in embryonic epidermal morphogenesis, we hypothesized that early loss of PAR3 could also result in disordered proliferation of these RAS-transformed cells.

Journal of Cell Science (2020) 133, jcs249102. doi:10.1242/jcs.249102

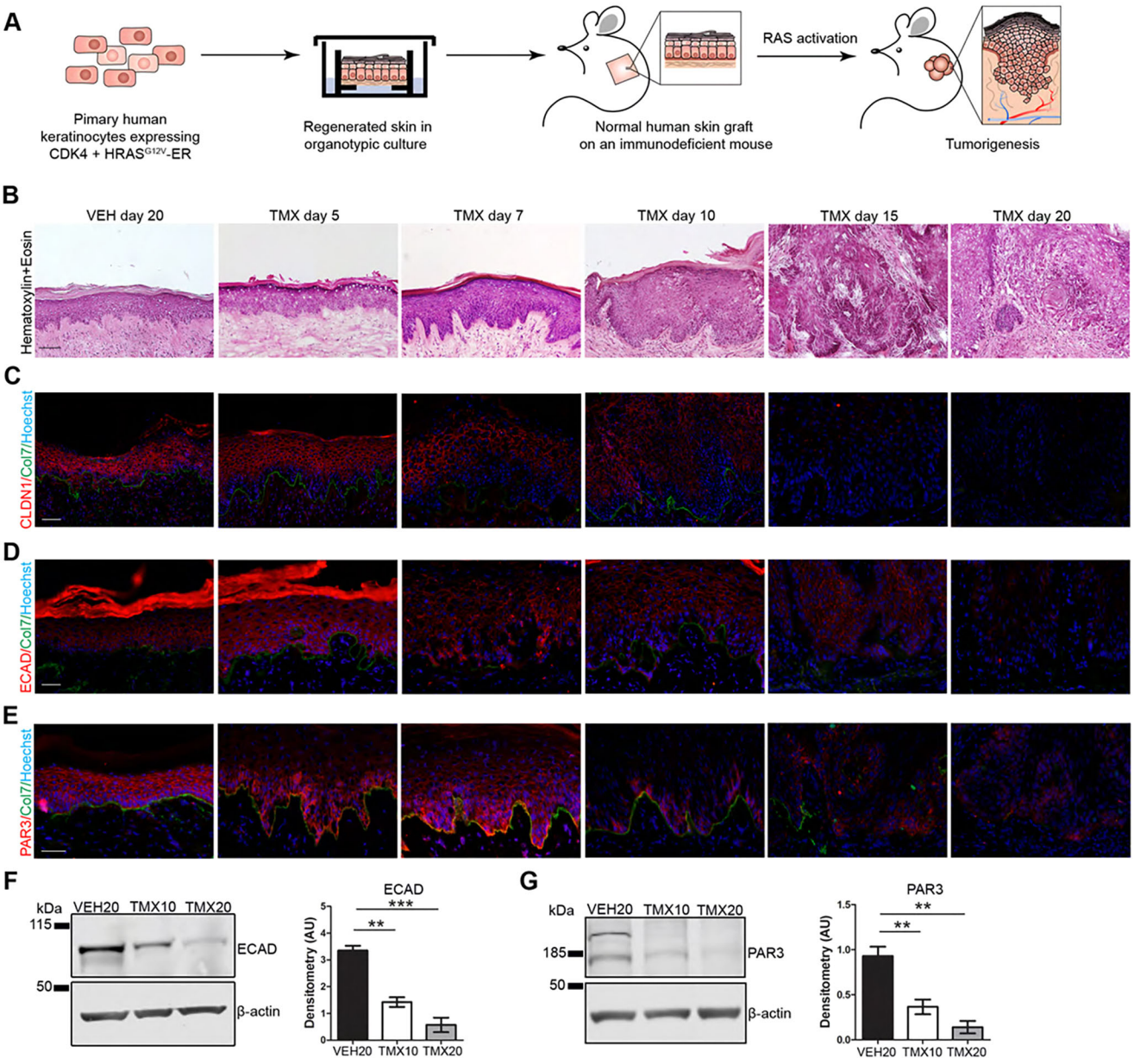

Fig. 1. Early transformation during human tumorigenesis is marked by hyperplasia and progressive loss of ECAD, CLDN1 and PAR3 protein. (A) Schematic of the inducible human epidermal neoplasia. CDK4 and tamoxifen (TMX)-inducible HRAS^{G12V} (RAS) is overexpressed in primary human keratinocytes. The genetically modified cells are seeded onto human devitalized dermis and stratified epidermis is formed in culture. The regenerated skin is transplanted onto an immunodeficient NSG mouse and the xenograft is allowed to heal for 2 weeks. Oncogenic HRAS is activated with daily injections of TMX, which leads to tumor formation. (B) H&E staining of CDK4/RAS regenerated epidermis at indicated number of days of TMX or vehicle (VEH) treatment. (C–E) Tissues from B were also immunostained with antibodies against CLDN1, ECAD and PAR3. All samples were co-stained with collagen VII (Col7) and Hoechst 33342 (nuclei). Images are representative of three or more xenografted animals analyzed per time point. Scale bars: 20 µm. (F,G) Western blot and densitometry analysis of (F) ECAD and (G) PAR3 protein expression in CDK4/RAS xenografts at indicated days of TMX or VEH treatment. *n*=3 animals. β-actin was used as loading control. Data represented as mean±s.e.m. ***P*<0.01; ****P*<0.001 (one-way ANOVA with Tukey test) relative to VEH.

To investigate oriented cell division, we stained normal and tumorigenic epidermis for phospho-histone H3 (pH3) to mark the directionality of cell division during tumor initiation. pH3 stains nuclei of actively dividing cells specifically in anaphase and telophase (where the outcome of cell division orientation has already been determined) (LaMonica et al., 2013; Miyashita et al., 2017; Zeng et al., 2007). Division planes were quantified by measuring the angle between the two daughter nuclei in relation to the basement membrane. Mitotic division angles (which indicate spindle orientation) between 0° and 20° were classified as planar, 20°–70° were defined as random, and 70°–90° were considered to be perpendicular (Fig. 3A). We also confirmed the efficacy of our method by labeling epidermal basal keratinocytes for survivin, a marker for late stage mitotic cells (Williams et al., 2011). Spindle orientations obtained from survivin staining were tightly correlated (R^2=0.936) with pH3 (Fig. S3A,B).

In normal human epidermis (VEH), we observed the majority of cell divisions to be either planar or perpendicular, as expected (Fig. 3B,C). Very few random orientations of the mitotic spindles were observed. However, this bimodal distribution of spindle

Journal of Cell Science (2020) 133, jcs249102. doi:10.1242/jcs.249102

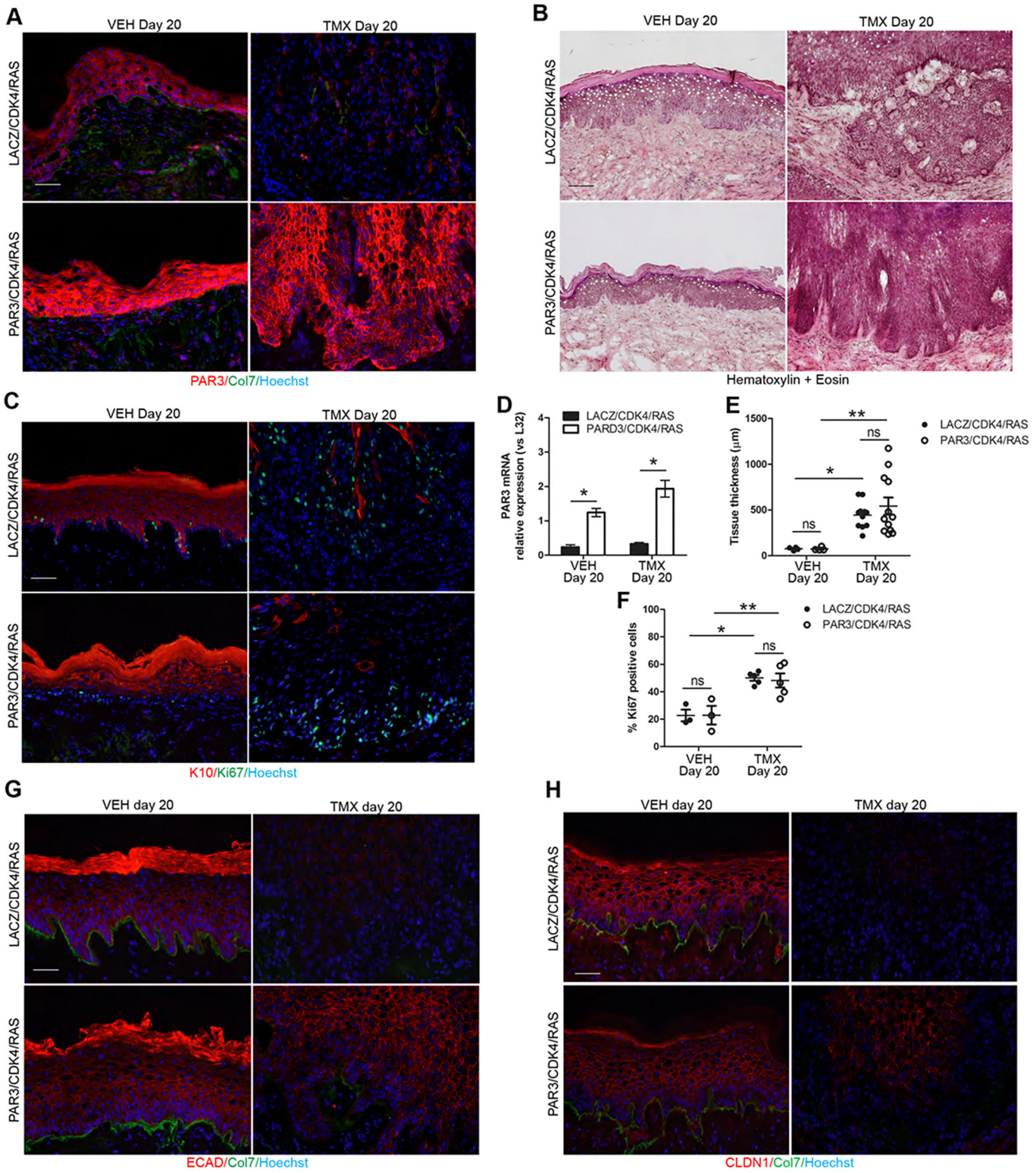

Fig. 2. PAR3 expression restores CLDN1 and ECAD-mediated formation of cell junctions. (A) LACZ or PAR3 ectopically expressed in CDK4/RAS xenografts and treated with VEH/TMX for 20 days. Representative images of PAR3 (red) and collagen VII (Col7, green) immunostaining are shown. Scale bar: 20 µm. *n*=3 animals per group. (B) H&E staining of LACZ/CDK4/RAS and PAR3/CDK4/RAS epidermis. (C) Immunostaining with the proliferation marker, Ki67 (green) and differentiation marker, K10 (red). (D) mRNA expression of PAR3 for the samples shown in A. **P*<0.05 (unpaired *t*-test). (E) Measurement of epidermal thickness. Each circle represents the average thickness of xenografted human skin from each individual mouse. *n*=4–12 xenografted mice analyzed per group. ***P*<0.01; ns, not significant (two-way ANOVA with Tukey test). (F) Quantification of the percentage of Ki67-positive cells for images shown in C. Each circle represents the average percentage of Ki6-positive cells from xenografted human skin from each individual mouse. *n*=3–5 mice analyzed per group. ***P*<0.01; ns, not significant (two-way ANOVA with Tukey test). (G) Representative images of ECAD (red) and collagen VII (Col7, green) immunostaining and (H) CLDN1 (red) and Col7 (green) immunostaining are shown. *n*≥3 xenografted animals analyzed per group for G and H. Scale bars: 20 µm. All data represented as mean±s.e.m.

Journal of Cell Science (2020) 133, jcs249102. doi:10.1242/jcs.249102

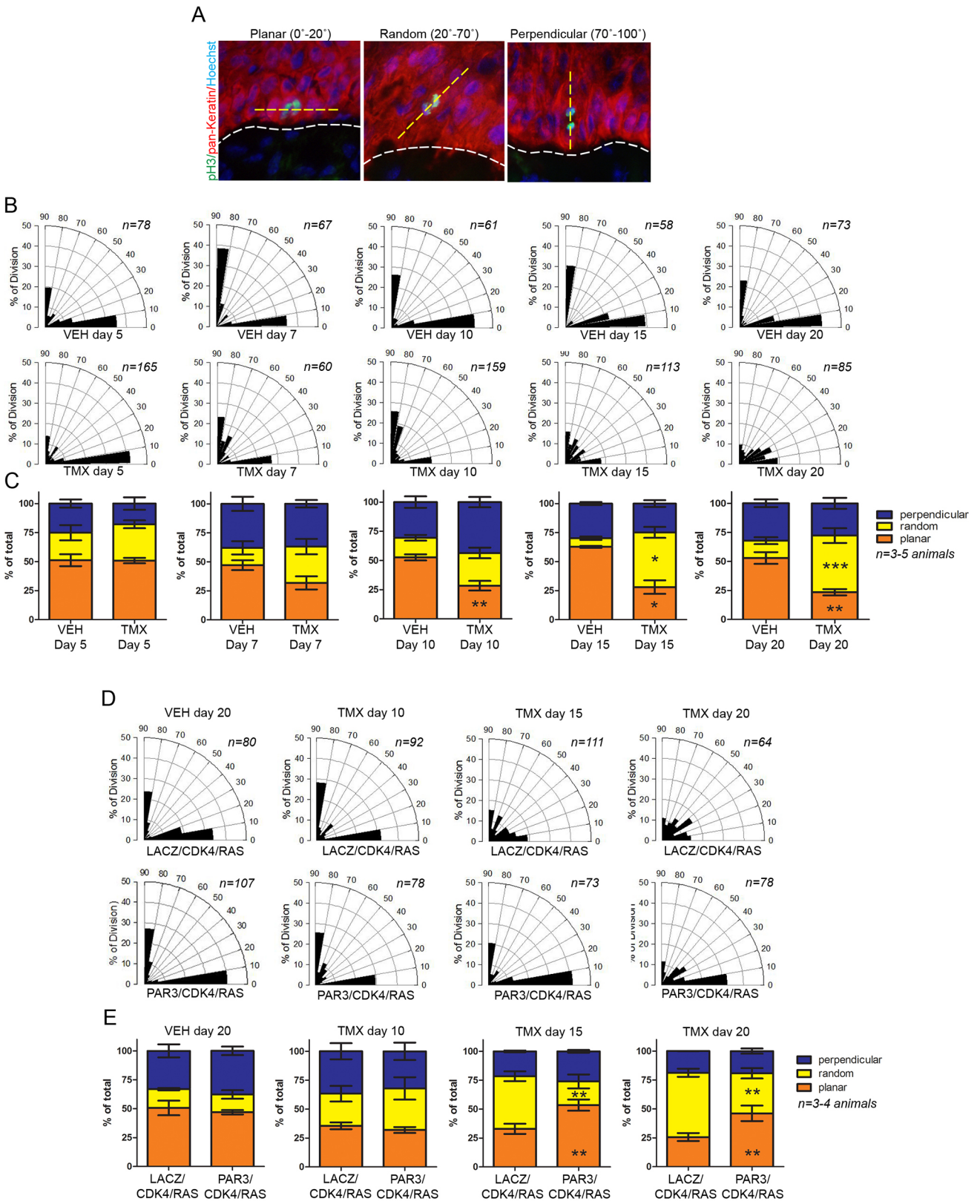

Fig. 3. See next page for legend.

orientation was progressively altered in TMX-treated tissues. A significant decrease in planar cell divisions was observed starting at day 10 of TMX treatment in comparison to VEH-treated epidermis (Fig. 3B,C). After 20 days of RAS activation, planar cell division only accounted for 25% of total cell divisions (vs 60% in VEH epidermis). Concurrently, there was a progressive increase in oblique/random cell divisions with RAS activation. By days 15 and 20, random divisions comprised the majority of the cell divisions

Fig. 3. Loss of oriented cell division during initial tumor growth can be restored with PAR3 expression. (A) Representative examples of cell division orientation in basal cells undergoing anaphase/telophase. Cells were labeled for phospho-histone 3 (pH3, green), pan-keratin (red), and Hoechst 33342 (nuclei; blue). Planar (0°–20°), random (20°–70°), and perpendicular (70°–90°) axes of cell division (dotted yellow line) were defined relative to the basement membrane (denoted by the dotted white line). (B) Radio histogram of cell division angles at indicated time points of TMX/VEH treatment in CDK4/RAS xenografts. *n*=number of spindles quantified for cell division orientation. (C) Statistical analysis of division angles at indicated time points aggregated from data in B. Cell division angles were combined from *n*=3–5 animals per group. **P*<0.05, ***P*<0.01, ****P*<0.001 (two-way ANOVA with Tukey test, relative to VEH-treated mice). (D) Frequency of basal cell division angels quantified from PAR3/CDK4/RAS and LACZ/CDK4/RAS grafts at indicated time points of TMX or VEH treatment. *n*=number of spindles quantified for cell division orientation. (E) Statistical analysis of division angles at indicated timepoints aggregated from data in D. Cell divisions were counted from 3–4 animals per group. ***P*<0.01 (two-way ANOVA with Tukey test, relative to LACZ/CDK4/RAS mice). All data represented as mean±s.e.m.

(50–60%) engaged by tumorigenic cells (Fig. 3B,C). Intriguingly, no changes to perpendicular cell division were observed with RAS activation (Fig. 3B,C). This dysregulation of cell division coincides with the loss of PAR3 expression and suggests that loss of PAR3-dependent cell polarity and the resulting changes in planar cell division are defining features of early tumorigenesis.

To support this hypothesis, we measured cell division orientation in TMX-induced PAR3/CDK4/RAS xenografts. As seen previously, RAS induction led to a progressive loss of planar division and corresponding increase in random divisions in control LACZ/CDK4/RAS tumors (Fig. 3D,E). In VEH PAR3/CDK4/RAS tissue, expression of PAR3 did not impact cell division orientation (Fig. 3D,E). In contrast, ectopic PAR3 expression in TMX-induced PAR3/CDK4/RAS xenografts prevented misorientation of cell division angles (Fig. 3D,E). After 20 days of TMX treatment, planar division still represented the majority of total cell division (∼50%), with random division comprising only of 25% of total cell division. This distribution mirrors what was observed in normal epidermis (i.e. VEH day 20; Fig. 3B,C) suggesting that ectopic expression of PAR3 can rescue the alterations in cell division orientation during tumor initiation (Fig. 3D,E). These results further strengthen our observation that PAR3 regulates cell division orientation in SCC tumor initiation and loss of PAR3 drives epidermal tissue disorganization.

ECAD depletion accelerates disordered cell division during tumorigenesis

Our temporal analysis of the RAS-induced SCC model demonstrated the importance of PAR3 levels on oriented cell division and its impacts on cell–cell junctions during early tumorigenesis. However, it is unclear whether these two processes are linked or if they are completely independent of one another. In simple epithelia, ECAD can direct mitotic spindle localization, as demonstrated in MDCK cells where selective loss of ECAD disrupted orientation of epithelial cell division (Gloerich et al., 2017). To address whether this can occur in stratified skin and in the context of tumor development, we decided to knockdown ECAD in CDK4/RAS xenografts (denoted shECAD/CDK4/RAS) to determine the effects of early disruption of ECAD-mediated junction formation on cell division orientation. We induced RAS activation in shECAD/CDK4/RAS and control (denoted shCtr/CDK4/RAS) xenografts for 5 days (Fig. 4A,B). This time point was chosen because no significant changes in tissue thickness, morphology, or proliferation were observed between shECAD/CDK4/RAS and shCtr/CDK4/RAS grafts (Fig. 4C–E). Furthermore, no difference was observed in PAR3, CLDN1 or ECAD expression or cell division orientation after 5 days of TMX treatment (vs VEH) in CDK4/RAS grafts (Figs 1C–E and 3B,C). Thus, if loss of ECAD cell–cell junctions is linked to regulation of cell division orientation, ECAD depletion would result in misorientation of cell division angles at an even earlier stage of tumor initiation. Indeed, shECAD/CDK4/RAS xenografts had significantly reduced planar cell divisions and increased random cell divisions within 5 days of TMX treatment (Fig. 4F,G). The distribution of cell division orientation observed in shECAD/CDK4/RAS tissues after 5 days of RAS activation resembles CDK4/RAS tissue after 15–20 days of TMX treatment. It is important to note that CLDN1 and PAR3 are still present and localized at appropriate cell junctions in 5 day-treated shECAD/CDK4/RAS xenografts (Fig. 4B). This suggests that ECAD-mediated junction formation alone can influence cell division orientation in stratified epithelium and PAR3 can work through ECAD to control planar cell divisions.

Inhibition of MAPK signaling restores PAR3 expression and function in RAS-activated tumors

Our results have demonstrated the crucial role of PAR3 in suppressing ECAD and CLDN1 cell–cell junction disruption and disordered cell division in early stages of RAS-dependent tumorigenesis. RAS can activate numerous downstream pathways, including MAPK, phosphoinositide-3 kinase (PI3K) and RalGEF pathways, to promote cancer (Rangarajan et al., 2004; Repasky et al., 2004). We hypothesized that RAS is directly reducing PAR3 levels through one of its numerous signaling pathways to disrupt cellular organization. Prior studies have identified the mitogen activated protein kinase (MAPK) cascade as a critical mediator of RAS-induced human skin tumorigenesis (Reuter et al., 2009; Ridky et al., 2010). Therefore, we hypothesized that RAS-dependent MAPK activation attenuates PAR3 protein expression, resulting in decreases in cell polarity, oriented cell division and CLDN1, ECAD cell junction assembly.

To investigate this possibility, mice implanted with TMX-activated CDK4/RAS xenografts were concomitantly treated with the MEK1/2 inhibitor U0126. Skin grafts were harvested after 20 days. U0126 treatment inhibited phosphorylation of ERK1 and ERK2 (ERK1/2, also known as MAPK3 and MAPK1, respectively), which are the downstream target of MEK1/2 in the MAPK pathway (Fig. 5A). Tissue thickness and proliferation (Ki67 positivity) was not significantly impacted as the epidermis was still hyperproliferative (Fig. 5B–E). However, blockade of the MAPK pathway restored PAR3 protein expression, as well as ECAD and CLDN1-mediated cell junction assembly (Fig. 5D,F). Additionally, random cell division angles were decreased from ∼50% in VEH-treated grafts to 25% in U0126-treated mice (Fig. 5G,H). This coincided with a gain in planar (∼50%) cell division angles in U0126-treated groups (Fig. 5G,H). This level of planar cell division is similar to that in normal epidermis (Fig. 3B,C) as well as 20 day TMX-treated PAR3/CDK4/RAS grafts (Fig. 3D,E). In summary, MAPK signaling downstream of RAS activation suppresses PAR3 protein levels, consequently disrupting PAR3-dependent downstream processes in organizing cell–cell contacts and cell division during cancer initiation (Fig. 6). Our results demonstrate that MAPK inhibitors can beneficially prevent deleterious dysregulation of cell and tissue organization in RAS-dependent SCC tumorigenesis.

DISCUSSION

Skin cancers are the most common type of cancer in the US with an estimated lifetime risk of one in five Americans contracting this

Journal of Cell Science (2020) 133, jcs249102. doi:10.1242/jcs.249102

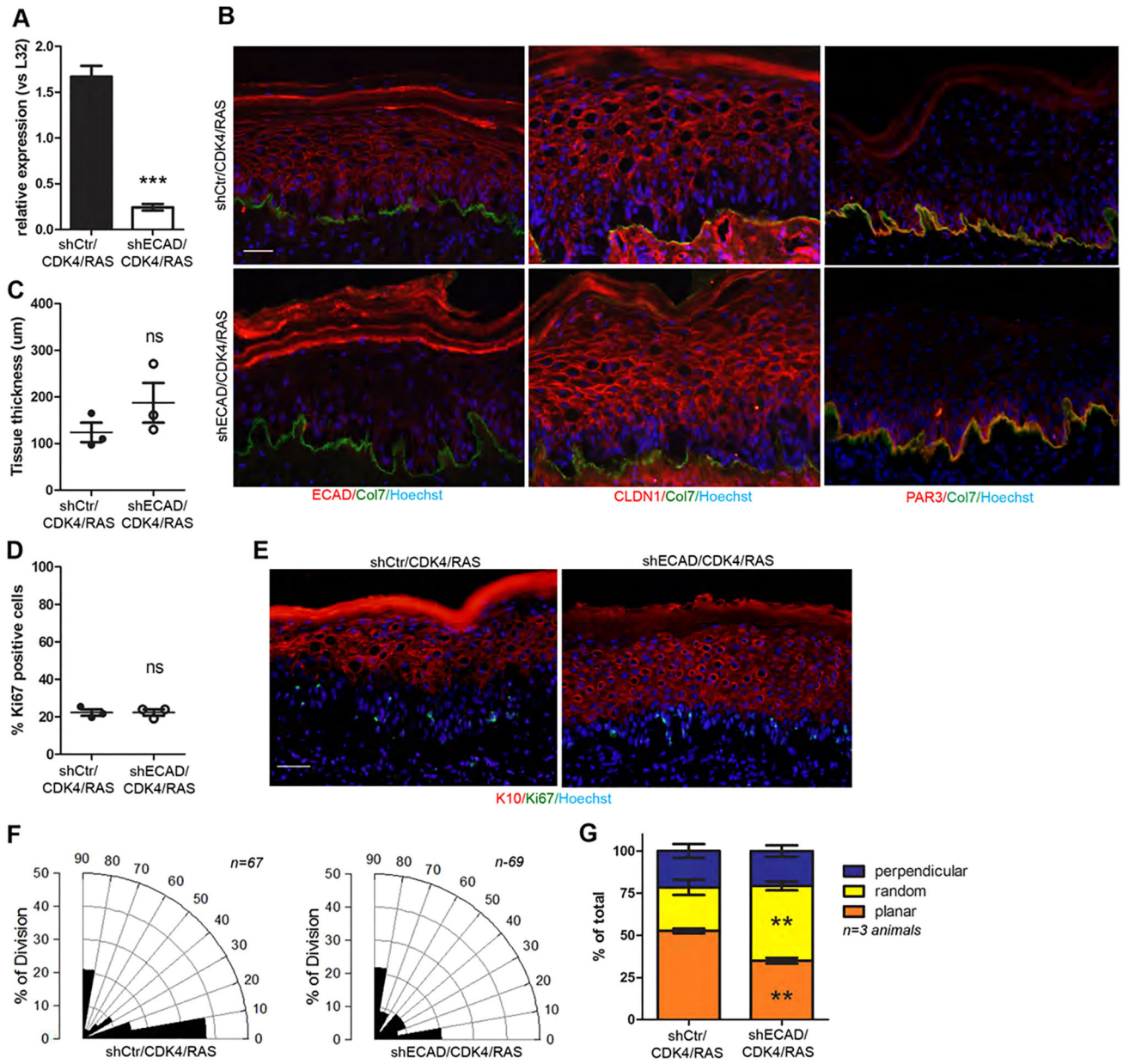

Fig. 4. E-cadherin loss accelerates disordered cell division. (A) Knockdown of ECAD (shECAD) or control knockdown (shCtr) in CDK4/RAS epidermis treated with TMX for 5 days. Quantification of ECAD mRNA expression was performed using RT-qPCR. *n*=3 grafts. ***P<0.001 (unpaired *t*-test). (B) Representative images of ECAD (red), CLDN1 (red), PAR3 (red), and collagen VII (Col7, green) immunostaining. Scale bar: 20 µm. (C) Epidermal thickness after 5 days of TMX treatment. Each circle represents the average epidermis thickness of an individual graft. *n*=3 mice analyzed per group. ns, not significant (unpaired *t*-test). (D) Quantification of percentage of Ki67-positive cells for images shown in E. *n*=3 mice analyzed per group. ns, not significant (unpaired *t*-test). (E) Immunostaining with the proliferation marker Ki67 (green) and differentiation marker K10 (red). Scale bar: 20 µm. (F) Radio histogram quantification of basal cell division angles after 5 days of TMX treatment. *n*=number of spindles quantified for cell division orientation. (G) Statistical analysis of cell division angles from data aggregated in F. *n*=3 xenografted mice analyzed per group. **P<0.01 (two-way ANOVA with Tukey test, relative to shCtr/CDK4/RAS tissue). All data represented as mean±s.e.m.

disease (Albert and Weinstock, 2003; Guy et al., 2015). The most prevalent oncogene mutated in skin carcinomas is RAS with 20% of SCCs associated with mutations in HRAS (Dotto and Rustgi, 2016; Pickering et al., 2014). Here, we investigate the timing of spindle misorientation in human oncogenic RAS dependent-SCC, and how deregulation of PAR3 expression affects tissue architecture and cell fate in relation to initial tumor formation. Prior *in vivo* analyses of potential oncogenes have primarily depended on mouse models (Gurumurthy and Lloyd, 2019; Khavari, 2006). However, genetically engineered mice are time-consuming to generate and are not amenable to combinatorial genetic or pharmacologic screens (Ridky et al., 2010). There are also vast differences in tissue morphology and gene expression between mouse and human skin (Khavari, 2006). Current techniques involving the ectopic injection of transformed primary human cells into the subcutaneous space of immuno-deficient mice, has offered a rapid high-throughput platform to assess the tumorigenic impact of specific genes (Elenbaas et al., 2001; Hahn et al., 1999). Nonetheless, tumor formation in this setting occurs in an environment not typically observed in human cancers (Khavari, 2006). The injected cells also develop in a space already lacking cell-to-basement membrane contacts and proper tissue architecture, which greatly hinders analysis of tissue disorganization during tumor formation.

Journal of Cell Science (2020) 133, jcs249102. doi:10.1242/jcs.249102

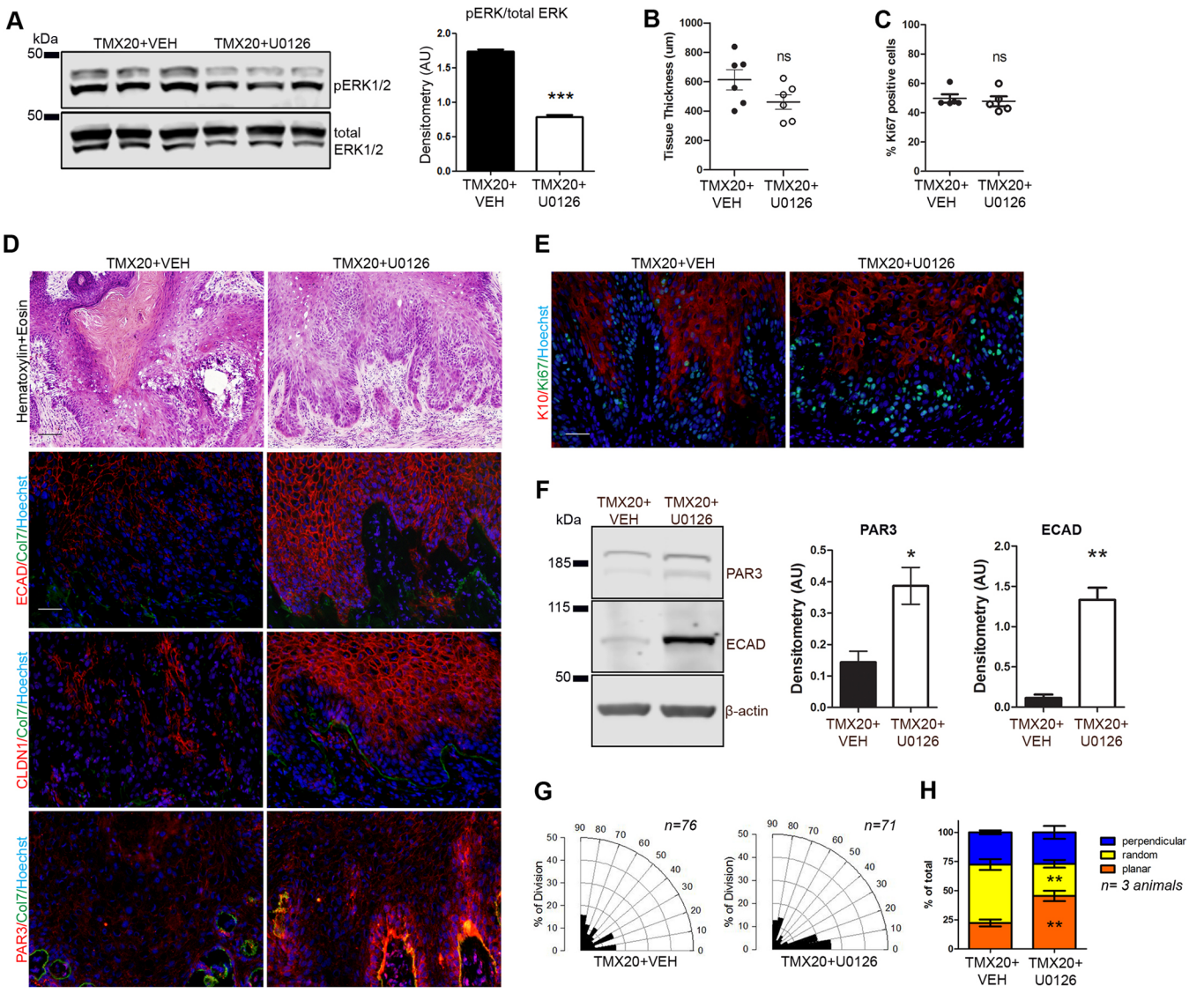

Fig. 5. Treatment with the MEK1/2 inhibitor U0126 restores PAR3 expression, cell junction formation, and oriented cell division. (A) Western blot analysis of tissue lysate isolated from CDK/RAS epidermis concomitantly treated with TMX and U0126 or VEH for 20 days (TMX20+U0126 and TMX20+VEH, respectively). Lysate was immunoblotted for phospho-ERK1/2 and total-ERK/2. Densitometry analysis was performed on n=3 animals per treatment. ***P<0.001 (unpaired t-test relative to TMX20+VEH). (B) Measurement of epidermal thickness. n=6 mice per group. ns, not significant (unpaired t-test). (C) Cell proliferation was measured as percentage of Ki67 positive cells in the basal epidermis. ns, not significant (unpaired t-test). (D) Representative image of H&E-stained tissue. TMX20+VEH and TMX20+U0126 xenografts were also stained with ECAD, CLDN1 and PAR3 antibodies. All immunofluorescence samples were co-stained with collagen VII (Col7) and Hoechst 33342 (nuclei). Scale bars: 20 µm. (E) Immunostaining for the proliferation marker, Ki67 (green), differentiation marker K10 (red) and Hoechst 33342 (nuclei). Scale bar: 20 µm. (F) Protein lysate isolated from TMX20+U0126- and TMX20+VEH-treated xenografts were blotted for PAR3 and ECAD expression. β-actin was used as loading control. Densitometry analysis based on n=3 animals per group. *P<0.05, **P<0.01 (unpaired t-test vs TMX20+VEH). (G) Radio histogram quantification of basal cell division angles of TMX20+VEH or TMX20+U0126 xenograft. n=number of spindles quantified for cell division orientation. (H) Statistical analysis of division angles expressed in G. n=number of xenografted animals analyzed per group. **P<0.01 (two-way ANOVA with Tukey test, relative to TMX20+VEH treated mice). All data represented as mean±s.e.m.

To examine neoplastic progression within an environment resembling native human skin tissue, we adapted a model previously published by Reuter et al. (2009). This model of TMX-inducible human neoplasia offers several advantages over established murine models. First, introduction of only two genes is needed to induce oncogenesis. We used mutant HRAS and CDK4 to mediate RAS pathway induction and bypass Rb (also known as RB1)-mediated G1 cell cycle restraints, which reflects alterations commonly observed in spontaneous human epithelial cancers (Ridky et al., 2010). Second, the transplanted skin xenograft exhibits 3D architecture phenotypic of normal human skin. This allows oncogenic transformation of normal epithelial cells to occur in an environment with established cell–cell adhesion, epithelial basement membrane and extracellular matrix (Lazarov et al., 2002; Reuter et al., 2009). Finally, transformation of keratinocytes with a TMX-inducible form of HRAS grants the investigator temporal control of tumor initiation. This enabled an in-depth characterization of cellular and molecular changes during initial stages of tumor formation, which was not possible with spontaneous tumor models. Using the original model, Reuter et al. analyzed gene expression profiles of both epithelia and stroma at specific time points during tumor progression. Our system differs from Reuter

Journal of Cell Science (2020) 133, jcs249102. doi:10.1242/jcs.249102

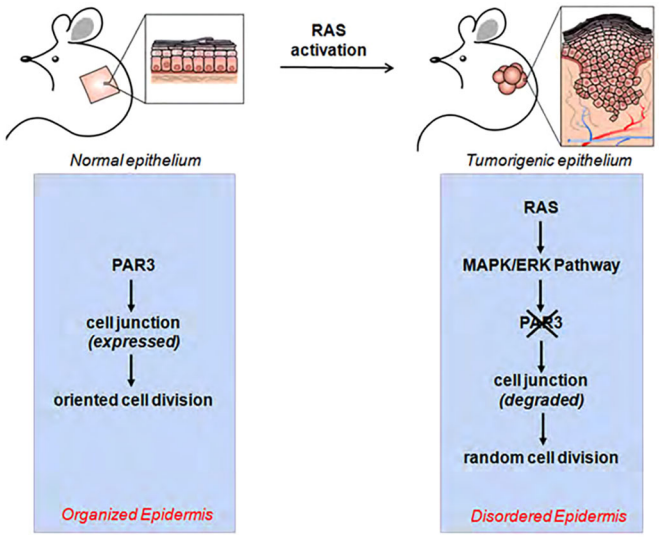

Fig. 6. Proposed model of how RAS-dependent suppression of PAR3 expression leads to loss of epithelial architecture during SCC formation. In normal epithelium, the presence of PAR3 promotes assembly of CLDN1- and ECAD-mediated cell junctions required for oriented cell divisions and normal epithelial architecture. In tumorigenic epithelium mediated by oncogenic RAS, activation of the MAPK/ERK pathway causes the depletion of PAR3, leading to the disassembly of CLDN1- and ECAD-mediated cell junctions, random cell divisions and a disorganized epithelium.

et al. in that our CDK4/HRAS xenografts (vs IκBα/HRAS xenografts used by Reuter et al.) were treated with TMX instead of 4-hydroxytamoxifen. Because 4-hydroxytamoxifen is 100× more bioactive than TMX (Katzenellenbogen et al., 1984; Robertson et al., 1982), Reuter et al. observed hyperplasia and disordered tissue architecture within 5 days of 4-hydroxytamoxifen treatment and invasion of epidermis into underlying stroma by day 20. This accelerated timeline prevented an examination of the mechanisms that lead to tissue disorganization. In contrast, our modifications resulted in a slower and less aggressive progression of tumorigenesis. Significant tissue hyerplasia was only observed after 15 days of TMX treatment and no invasive phenotypes were observed after 20 days of TMX injection. Moreover, changes in tissue architecture took place over a period of 20 days rather than 5 days, which allowed dissection of the pathway important for this process. Overall, our model allowed for gradual transformation of normal human keratinocytes and the initial cellular changes observed during tumorigenesis are likely to be more indicative of the early stages of oncogenic activation than prior studies. To our knowledge, this is the first temporal documentation of spindle orientation deregulation and loss of ECAD- and CLDN1-mediated cell junction formation in RAS-driven tumorigenesis in 3D intact human skin.

In our efforts to catalog the initial molecular events of RAS-driven SCC, we discovered that attenuation of PAR3 expression was a determining cause of tissue disorganization during RAS-dependent tumor development. PAR3 has also been studied in mouse skin tumors where PAR3 knockout mice inhibited DMBA/TPA mediated formation of skin papillomas (Iden et al., 2012). In that context, PAR3 was found to localize to cell–cell junctions and to be necessary for assembling Ras and its effectors, Sos2 and ERK1/2 at intercellular contacts to promote growth and survival signaling. The authors also observed an increase in keratoacanthoma formation in the DMBA/TPA-treated PAR3 knockout mice. In a follow-up study, these authors found that PAR3 knockout DMBA/TPA-treated mice also had increased invasion and tissue disorganization during the late stages of carcinogenesis (Vorhagen et al., 2018). These studies illustrate the complex roles that PAR3 may play in tumorigenesis where in the early stages it can cooperate with Ras to promote tumor initiation while in the later stages it inhibits invasion. Our studies are consistent with the latter stages of tumor formation in the mouse model since our human model directly progresses to SCCs. Our findings also illustrate a pathway in which RAS-mediated downregulation of PAR3 results in loss of ECAD from cell junctions, leading to disordered cell division. We believe this is the first demonstration of the essential role of PAR3 and ECAD have in maintaining tissue architecture during SCC tumor initiation. Downregulation of PAR3 and ECAD have been associated with the later stages of tumor progression, notably in breast and lung cancer (Bonastre et al., 2015; McCaffrey et al., 2016). However, in both cases, increased cell migration was postulated to be the cause of the observed metastasis. Taken in combination with our data, it is likely that continued downregulation of PAR3 and ECAD are required for tumor invasiveness during SCC development. Future experiments are required to address this. In models of single-layered epithelium, ECAD has also been shown to direct mitotic spindle by providing anchoring and spatial cues for LGN (also known as GPSM2) (Anastasiou et al., 2020; Gloerich et al., 2017; Hart et al., 2017; Wang et al., 2018). In murine skin, adherens junction proteins such as afadin, vinculin and αE-catenin correct random angle divisions during telophase through an LGN-independent process to generate proper tissue organization (Lough et al., 2019). While our data supports a role for ECAD in regulating oriented cell divisions in stratified human skin, further investigation is needed to determine whether ECAD is acting through an LGN-independent or -dependent process to promote spindle orientation and tissue organization.

In addition to tissue organization, oriented cell division can also control cell fate specification (Žigman et al., 2005). Unbalanced inheritance of cytosolic content, as well as exposure to different environments, can greatly influence the identity and function of the daughter cells (Neumüller and Knoblich, 2009). Interestingly, loss of PAR3 directed cell division during RAS-induced tumorigenesis does not affect cell fate determination. We showed that restoring PAR3 expression during RAS activation had no effect on the proliferative phenotype, despite normalizing distribution of cell division angles. Given that random divisions may function similarly to planar ones, our findings suggest that loss of PAR3 promotes neoplasic progression of SCC through tissue disorganization rather than cell fate choices.

Regulators of cell polarity have long been recognized as a determinant of cell division orientation in *C. elegans* zygotes and *Drosophila* neuroblasts (Goldstein and Macara, 2007). In mouse embryonic epidermis, the apicobasal regulator PAR3 has been shown to localize LGN to the apical cortex, which facilitates mitotic spindle alignment perpendicular to the basal membrane (Lechler and Fuchs, 2005; Williams et al., 2014). The resulting asymmetric cell division is integral in the formation of stratified epidermis as it generates a progenitor cell and a daughter cell committed to differentiation. However, PAR3 knockout had no significant impacts on cell division angles in adult mice interfollicular epidermis (Ali et al., 2016). Our study demonstrates that decreased PAR3 levels results in loss of planar cell division in human epidermis during RAS-induced tumorigenesis while not affecting perpendicular cell division. It is possible that in our tumor model PAR3 does not directly regulate cell division orientation as opposed to what has been demonstrated for the direct role of PAR3 in promoting perpendicular cell divisions in mouse embryonic epidermis (Williams et al., 2014). This may be the case, as indicated

Journal of Cell Science (2020) 133, jcs249102. doi:10.1242/jcs.249102

by the following observations: (1) PAR3 overexpression results in oblique angle divisions being converted into planar ones rather than perpendicular ones; (2) PAR3 overexpression restores ECAD to cell junctions; and (3) ECAD depletion by shRNAs at day 5 of RAS activation leads to significant loss of planar divisions and a gain in oblique/random divisions. This mimicked the division angles of much more advanced tumors, such as those at days 15 and 20 of RAS activation. Knockdown of ECAD also did not perturb PAR3 or CLDN1 at cell junctions, suggesting a direct role for ECAD in mediating cell division orientation. Thus, our studies, in combination with others, suggest that PAR3-driven regulation of oriented cell division may be context dependent.

PAR3 expression, which we have now shown to be essential for directed cell division in human SCC, is lost or significantly reduced in several human malignancies (Bonastre et al., 2015; Guo et al., 2016; McCaffrey et al., 2016; Zhang et al., 2019). PAR3 mutations were also detected in 30% of patients with aggressive SSC (Pickering et al., 2014). Furthermore, loss of epidermal PAR3 in mice also led to melanocyte hyperplasia and increased tumor formation due to upregulation of P-cadherin (Mescher et al., 2017). Although these studies have correlated PAR3 expression loss with malignant progression, the precise mechanism by which PAR3 expression is altered during tumor development has never been investigated. Our results indicate that a pathway downstream of RAS signaling is responsible for downregulating PAR3 protein levels. One such pathway, the MAPK cascade is mutated in 30% of all cancers and is the most frequently activated pathway in SCC (Cheng and Tian, 2017; Dajee et al., 2003). In recent years, it has become a promising target for cancer therapy due to its ascribed roles in proliferation, differentiation and survival (Cheng and Tian, 2017). Genetic ablation of MAPKKs (MEK1/2) in mouse epidermis resulted in defects in barrier function due to hypoproliferation and increased apoptosis, and loss of MEK1 reduced tumor formation in DMBA/TPA-induced mouse skin carcinoma (Scholl et al., 2007, 2009). To determine whether the MAPK pathway regulates PAR3 expression in our model of RAS-induced human SCC, we pharmacologically treated mice with U0126, a specific inhibitor of MEK1/2 (Favata et al., 1998). PAR3 expression, ECAD-mediated cell junction assembly and oriented cell divisions were all restored upon MEK1/2 inhibition. Importantly, tissue growth was not affected by U0126 treatment, providing evidence that the primary role of the MAPK/ERK pathway in our human xenograft model is not the control of cell proliferation but rather the regulation of PAR3 protein and its associated functions during initiation of RAS-activated SCCs. Our results demonstrate that activation of the MAPK pathway regulates PAR3 expression and localization to cell junctions; however, the precise mechanism of how this is done is not clear. A previous study has shown that ERK2 directly interacts and phosphorylates PAR3 at Ser-1116 in neurons (Funahashi et al., 2013). This results in the accumulation of PAR3 at axonal tips. ERK1/2 has also been shown to be necessary for the proteasome-dependent degradation of proteins involved in promoting cell cycle and migration through phosphorylation of its target proteins (Deschenes-Simard et al., 2013). Thus, it is possible that ERK2 phosphorylates PAR3 in our tumor model to cause its degradation.

In conclusion, our use of an inducible model of *in vivo* human neoplasia to evaluate molecular changes driving tumorigenesis complements other efforts using mice or *in vitro* cancer cell models. However, our approach differs from those in previous studies in that we were able to analyze the temporal progression of tissue disorganization during the initial stages of human SCC development *in vivo*. As a result, we were able to demonstrate how loss of PAR3 protein can potentiate SCC tumorigenesis via increased tissue disorganization, but not cell fate determination, in a setting that phenotypically mimics human epithelial structure. It will be important in the future to determine the extent to which PAR3 loss leads to altered division angles and disrupted tissue architecture in spontaneous human SCCs. It will also be interesting to assess whether this also correlates with the progression of the tumor from pre-cancerous to invasion. Finally, we elucidated a novel MAPK-dependent regulation of PAR3 protein expression, which can be reversed by *in vivo* administration of the MAPK inhibitor, U0126. Therefore, our use of inducible SCC transformation of primary human keratinocytes improves upon previous cancer models by providing a more-relevant system to answer basic questions about oncogenesis, and a platform that is amenable to assessing relevant pharmacological interventions *in vivo*.

MATERIALS AND METHODS

Cell culture

Primary human epidermal keratinocytes purchased from Life Technologies (Thermo Fisher Scientific; C0015C) and were derived from neonatal foreskin and cultured in EpiLife medium (Thermo Fisher: MEPI500CA) and human keratinocyte growth supplement (HKGS, Thermo Fisher: S0015) as previously described (Mistry et al., 2012; Sen et al., 2010; Wang et al., 2015). Phoenix cells (ATCC CRL-3214) were cultured in DMEM with 10% fetal bovine serum. All cells were maintained in a 37°C, 5% CO_2 incubator.

Gene silencing

To achieve stable knockdown of ECAD in primary human keratinocytes, shRNAs targeting ECAD were first cloned into the pSuper retroviral vector (Sen et al., 2004). The resulting retroviral construct (3 µg) were then transfected into amphotropic phoenix cells using Lipofectamine 2000 (Life Technologies: 11668027). Supernatants containing the retrovirus were collected at 48 h post transfection and used to infect primary human keratinocytes. Infection of the keratinocytes occurred over 2 consecutive days. Each day, the viral supernatant, plus 5 µg/ml polybrene (Sigma-Aldrich; H9268), were placed on the cells and centrifuged at 1700 ***g*** for 1 h. Selection of infected cells occurred in medium supplemented with 1 µg/ml puromycin. The shRNA sequence targeting ECAD is 5′-GCACCACTAC-GCATGACTA-3′. The control shRNA construct was generated as previously described (Sen et al., 2010).

Gene overexpression

Retroviral constructs for tamoxifen-reponsive ER-HRAS^{G12V}, CDK4 and PAR3 were generated and stable cell lines of amphotropic phoenix cells expressing each of the above retroviral constructs were made. Viral supernatants were collected from the stable cell lines and used to infect primary human keratinocytes as described in the ‘Gene silencing’ section above. The LZRS-PAR3 construct was made by cloning the full-length open reading frame of PAR3 into the LZRS retroviral vector using the restriction enzymes HindIII and NotI. The primers used to amplify PAR3 were: PAR3 forward, 5′-ACGCAAAGCTTGCCACCATGAAAGTGACCGTGTGCT-TCGGACGGACCCGGGTGGTCG-3′ and PAR3 reverse, 5′-ACGCAGC-GGCCGCTCAGGAATAGAAGGGCCTCCCTTTCTCAGGAGTCTGA-AGT-3′. The LZRS-CDK4 and LZRS-ER-HRAS retroviral constructs were generous gifts from the Khavari laboratory (Department of Dermatology, Stanford University, CA, USA) (Lazarov et al., 2002; Reuter et al., 2009).

Gene expression analysis

Total RNA was purified from cells and tissue using Trizol and Direct-zol RNA purification kit (Zymo Research: R2051) according to manufacturer’s instructions. RNA was quantified using a Nanodrop. A total of 1 µg of total RNA was reversed transcribed using the Maxima cDNA synthesis kit (Thermo Fisher: K1642) and quantitative PCR was performed using the

Bio-Rad CFX96 machine. *L32* was used as internal control for normalization. Sequence of primers used are as follows: L32 forward, 5′-AGGCATTGACAACAGGGTTC-3′, L32 reverse, 5′-GTTGCACATCA-GCAGCACTT-3′; KRT2 forward, 5′-GCTTTGGCAGTCGGAGTC-3′, KRT2 reverse, 5′-CTCCACCGAAACCACCAC-3′; MMP1 forward, 5′-TGGACCATGCCATTGAGA-3′, MMP1 reverse, 5′-TACCTGGGC-CTGGTTGAA-3′; ITGB1 forward, 5′-AATGCCAAATGGGACACG-3′, ITGB1 reverse, 5′-TTGCACGGGCAGTACTCA-3′; VEGFC forward, 5′-GAAAGGAGGCTGGCAACA-3′, VEGFC reverse, 5′-TG-TTTGTCGCGACTCCAA-3′; PAR3 forward, 5′-CCATGCGTACACC-CATCA-3′, PAR3 reverse, 5′-TTCAGTCGGGGTGCTCTC-3′; CLDN1 forward, 5′-GTCATTGGGGGTGCGATA-3′, CLDN1 reverse, 5′-CA-CCTCCCAGAAGGCAGA-3′; ECAD forward, 5′-GGCCTCCGTTTC-TGGAAT-3′, ECAD reverse, 5′-TCCTTGGCCAGTGATGCT-3′; CDK4 forward, 5′-GCTGCCTCCAGAGGATGA-3′, CDK4 reverse, 5′-GCTGCAGAGCTCGAAAGG-3′; SNAIL forward, 5′-TTCCAGC-AGCCCTACGAC-3′, SNAIL reverse, 5′-CAGGGAGGTCAGCTCTG-C-3′; SLUG forward, 5′-CACCTCCTCCAAGGACCA-3′, SLUG reverse, 5′-GGCCAGCCCAGAAAAAGT-3′; TWIST2 forward, 5′-TCCAGCAACTCCGAGAGC-3′, TWIST2 reverse, 5′-GCCTCTC-GAGCTCCTCCT-3′; AREG forward, 5′-TACTCGGCTCAGGCCATT-3′, AREG reverse, 5′-CCCGAGGACGGTTCACTA-3′; EREG forward, 5′-AACCGTCCACCAACCTTT-3′, EREG reverse, 5′-CTTGCGGCA-ACTCTGGA-3′.

Animal studies

3D organotypic skin was generated by seeding 10^6 genetically modified primary human keratinocytes onto devitalized human dermis as previously described (Li et al., 2019; Li and Sen, 2015; Wang et al., 2015). The tissue was grown in an air–liquid interface over 7 days, before being grafted onto male and female immunodeficient NOD scid gamma (NSG) mice (Jackson Labs) of 12–16 weeks of age. The xenografts were allowed to heal for 2 weeks before bandages and sutures were removed. Immediately after, RAS activation was induced by daily intraperitoneal (IP) injections of TMX (Sigma Aldrich; 1.12 mg) which was resuspended in 10% ethanol and corn oil (Reuter et al., 2009). Vehicle-treated animals were injected daily with 10% ethanol and corn oil without TMX. Animals were harvested after vehicle or TMX treatment for 5, 7, 10, 15 and 20 days after the start of IP injections. Harvested tissue was placed in OCT for immunostaining or snap frozen in liquid nitrogen to be used later for protein or RNA expression analysis. All animal work was done in accordance with, and approved by, the University of California, San Diego's Institutional Animal Care and Use Program.

U0126 treatment

MEK inhibitor U0126 (Cell Signaling, #9903) was reconstituted in 2.5% DMSO, 30% Kolliphor EL (Sigma C5135), 10% ethanol and PBS. U0126 solution was IP injected daily (0.2 mg per mouse) in conjunction with TMX. 2.5% DMSO, 30% Kolliphor EL, 10% ethanol and PBS were used as vehicle control. Tissues were harvested after 20 days of treatment with U0126 and TMX.

Western blotting

Frozen tissue was homogenized in RIPA buffer (Thermo Fisher, 89900) containing phosphatase (Thermo Fisher, A32957) and protease inhibitor (Sigma-Aldrich, 11836170001) using the Bullet Blender tissue homogenizer. Protein concentration of the lysate was determined using BCA protein assay kit (Thermo Fisher, 23225). 60 µg of protein per sample was resolved by SDS-PAGE and transferred to nitrocellulose membranes. Membranes were blocked in 3% BSA plus 0.5% Tween 20 in TBS and incubated in primary antibody overnight at 4°C. The primary antibodies used were against the following proteins: phospho-p44/42 MAPK (ERK1/2, Cell Signaling, 4370) at 1:1000, p44/42 MAPK (ERK1/2; Cell Signaling, 4695) at 1:1000, β-actin (Santa Cruz Biotechnology, SC-47778) at 1:5000, PAR3 (Novus Biological, NBP188861) at 1:500, ECAD (Cell Signaling, 3195) at 1:1000, SLUG (Cell Signaling, 9585) 1:500, and SNAIL (Cell Signaling, 3879) at 1:500. After washing, membranes were incubated with secondary antibody, and visualized with LICOR. The secondary antibodies used were IRDye 680RD Donkey anti-rabbit IgG (LICOR: 926-68073) at 1:10,000 and IRDye 800CW donkey anti-mouse IgG (LICOR: 926-32212) at 1:10,000.

Immunostaining

For immunofluorescence staining of cryosectioned tissue, cryostections (5–7 µm) were fixed (10% buffered formalin, methanol plus 5% acetic acid or acetone), blocked in 2.5% goat serum, 0.3% Triton X-100 and 3% bovine serum in PBS, and incubated with primary antibody (diluted in blocking buffer) overnight at 4°C. The primary antibodies used were against: K10 (Abcam, AB9025) at 1:500, Collagen VII (Santa Cruz Biotechnology, SC33710) at 1:100, KI67 (Abcam, AB16667) at 1:300, PAR3 (Novus Biological, NBP188861) at 1:100, CLDN1 (Thermo Fisher, 71-7800) at 1:100, ECAD (Cell Signaling, 3195) at 1:100, phospho-histone3 (pH3; Cell Signaling, 9706) at 1:250, and survivin (Cell Signaling, 2808) at 1:400. Bound primary antibody was detected by fluorescent-dye-conjugated secondary antibodies. These secondary antibodies include: Alexa Fluor 555-conjugated goat anti-mouse IgG (Thermo Fisher: A11029) at 1:500, Alexa Fluor 488-conjugated donkey anti-rabbit IgG (Thermo Fisher, A21206) at 1:500, Alexa Fluor 555-conjugated goat anti-rabbit IgG (Thermo Fisher: A21429) at 1:500, Alexa Fluor 488-conjugated goat anti-mouse IgG (Thermo Fisher, A11001) at 1:500. The nuclei were counterstained with Hoechst 33342 in PBS (1:1000, Thermo Fisher, H3570). After washing with PBS, slides were mounted in Fluoromount (Thermo Fisher, 00-4958-02). Images were taken with an Olympus Dx71 camera mounted to a fluorescence microscope.

Histological analysis

Cryosections cut at 20 µm were stained with hematoxylin and eosin (H&E). Images were taken with an Olympus DP71 camera attached to an Olympus BX51 microscope. Epidermal thickness was measured at the thickest region of each section, from the base to the top of the epidermis using ImageJ software. Three independent measurements were performed for each group at each time point.

Measurement of cell division angles

Cell division orientation was determined as described previously (Williams et al., 2014). Cryosections (5 µm) were stained with pH3 to detect cells in anaphase/telophase. Sections were co-stained with a pan-keratin antibody (Biolegend, PRB-160P) at 1:500 to differentiate the epidermis and dermis boundary, which allows identification of the basement membrane. The angle of cell division was assessed by measuring the angle of the plane transecting two dividing nuclei relative to the plane of the basement membrane. Divisions were categorized as either symmetric (0°–20°), oblique (20°–70°), or asymmetric (70°–90°) and plotted in radial histograms using Origin 2016 (OriginLab). The number of dividing cells analyzed is indicated in the radial histogram. The number of analyzed cells comes from 3 or more mice per group per time point.

Statistical analysis

All data are presented as mean±s.e.m. and analyzed using Graphpad Prism. Statistical significance was assessed using two-way ANOVA when comparing multiple treatments between two or more groups, one-way ANOVA when comparing multiple treatments within a single group or an unpaired *t*-test when comparing two treatments. $P<0.05$ was considered statistically significant.

Acknowledgements

We would like to thank the Khavari lab for the LZRS-CDK4 and LZRS-RAS-ER retroviral constructs used in this study.

Competing interests

The authors declare no competing or financial interests.

Author contributions

Conceptualization: J. Ling; Methodology: J. Ling, M.S., M.T., Y.C.; Software: J. Ling; Validation: J. Ling, M.S., M.T.; Formal analysis: J. Ling; Investigation: J. Ling, M.S., M.T., Y.C.; Data curation: J. Ling; Writing - original draft: J. Ling, G.L.S.; Writing - review & editing: J. Ling, M.S., M.T., Y.C., J. Li, J.J., G.L.S.; Supervision: G.L.S.; Project administration: G.L.S.; Funding acquisition: G.L.S.

Funding
This work was supported by grants from the National Institutes of Health (NIH R01AR072590 and R01CA225463) to G.L.S. Deposited in PMC for release after 12 months.

Supplementary information
Supplementary information available online at
https://jcs.biologists.org/lookup/doi/10.1242/jcs.249102.supplemental

Peer review history
The peer review history is available online at
https://jcs.biologists.org/lookup/doi/10.1242/jcs.249102.reviewer-comments.pdf

References

Albert, M. R. and Weinstock, M. A. (2003). Keratinocyte carcinoma. *CA Cancer J. Clin.* **53**, 292-302. doi:10.3322/canjclin.53.5.292
Ali, N. J. A., Dias Gomes, M., Bauer, R., Brodesser, S., Niemann, C. and Iden, S. (2016). Essential role of polarity protein Par3 for epidermal homeostasis through regulation of barrier function, keratinocyte differentiation, and stem cell maintenance. *J. Invest. Dermatol.* **136**, 2406-2416. doi:10.1016/j.jid.2016.07.011
Anastasiou, O., Hadjisavva, R. and Skourides, P. A. (2020). Mitotic cell responses to substrate topological cues are independent of the molecular nature of adhesion. *Sci. Signal.* **13**, eaax9940. doi:10.1126/scisignal.aax9940
Bergstralh, D. T., Dawney, N. S. and St Johnston, D. (2017). Spindle orientation: a question of complex positioning. *Development* **144**, 1137-1145. doi:10.1242/dev.140764
Bonastre, E., Verdura, S., Zondervan, I., Facchinetti, F., Lantuejoul, S., Chiara, M. D., Rodrigo, J. P., Carretero, J., Condom, E., Vidal, A. et al. (2015). PARD3 inactivation in lung squamous cell carcinomas impairs STAT3 and promotes malignant invasion. *Cancer Res.* **75**, 1287-1297. doi:10.1158/0008-5472.CAN-14-2444
Box, K., Joyce, B. W. and Devenport, D. (2019). Epithelial geometry regulates spindle orientation and progenitor fate during formation of the mammalian epidermis. *eLife* **8**, e47102. doi:10.7554/eLife.47102
Cheng, Y. and Tian, H. (2017). Current development status of MEK inhibitors. *Molecules* **22**, 1551. doi:10.3390/molecules22101551
Dajee, M., Lazarov, M., Zhang, J. Y., Cai, T., Green, C. L., Russell, A. J., Marinkovich, M. P., Tao, S., Lin, Q., Kubo, Y. et al. (2003). NF-κB blockade and oncogenic Ras trigger invasive human epidermal neoplasia. *Nature* **421**, 639-643. doi:10.1038/nature01283
Deschenes-Simard, X., Gaumont-Leclerc, M.-F., Bourdeau, V., Lessard, F., Moiseeva, O., Forest, V., Igelmann, S., Mallette, F. A., Saba-El-Leil, M. K., Meloche, S. et al. (2013). Tumor suppressor activity of the ERK/MAPK pathway by promoting selective protein degradation. *Genes Dev.* **27**, 900-915. doi:10.1101/gad.203984.112
di Pietro, F., Echard, A. and Morin, X. (2016). Regulation of mitotic spindle orientation: an integrated view. *EMBO Rep.* **17**, 1106-1130. doi:10.15252/embr.201642292
Dotto, G. P. and Rustgi, A. K. (2016). Squamous cell cancers: a unified perspective on biology and genetics. *Cancer Cell* **29**, 622-637. doi:10.1016/j.ccell.2016.04.004
Elenbaas, B., Spirio, L., Koerner, F., Fleming, M. D., Zimonjic, D. B., Donaher, J. L., Popescu, N. C., Hahn, W. C. and Weinberg, R. A. (2001). Human breast cancer cells generated by oncogenic transformation of primary mammary epithelial cells. *Genes Dev.* **15**, 50-65. doi:10.1101/gad.828901
Favata, M. F., Horiuchi, K. Y., Manos, E. J., Daulerio, A. J., Stradley, D. A., Feeser, W. S., Van Dyk, D. E., Pitts, W. J., Earl, R. A., Hobbs, F. et al. (1998). Identification of a novel inhibitor of mitogen-activated protein kinase kinase. *J. Biol. Chem.* **273**, 18623-18632. doi:10.1074/jbc.273.29.18623
Funahashi, Y., Namba, T., Fujisue, S., Itoh, N., Nakamuta, S., Kato, K., Shimada, A., Xu, C., Shan, W., Nishioka, T. et al. (2013). ERK2-mediated phosphorylation of Par3 regulates neuronal polarization. *J. Neurosci.* **33**, 13270-13285. doi:10.1523/JNEUROSCI.4210-12.2013
Gillies, T. E. and Cabernard, C. (2011). Cell division orientation in animals. *Curr. Biol.* **21**, R599-R609. doi:10.1016/j.cub.2011.06.055
Gloerich, M., Bianchini, J. M., Siemers, K. A., Cohen, D. J. and Nelson, W. J. (2017). Cell division orientation is coupled to cell-cell adhesion by the E-cadherin/LGN complex. *Nat. Commun.* **8**, 13996. doi:10.1038/ncomms13996
Goldstein, B. and Macara, I. G. (2007). The PAR proteins: fundamental players in animal cell polarization. *Dev. Cell* **13**, 609-622. doi:10.1016/j.devcel.2007.10.007
Guo, X., Wang, M., Zhao, Y., Wang, X., Shen, M., Zhu, F., Shi, C., Xu, M., Li, X., Peng, F. et al. (2016). Par3 regulates invasion of pancreatic cancer cells via interaction with Tiam1. *Clin. Exp. Med.* **16**, 357-365. doi:10.1007/s10238-015-0365-2
Gurumurthy, C. B. and Lloyd, K. C. K. (2019). Generating mouse models for biomedical research: technological advances. *Dis. Model. Mech.* **12**, dmm029462. doi:10.1242/dmm.029462
Guy, G. P., Jr., Machlin, S. R., Ekwueme, D. U. and Yabroff, K. R. (2015). Prevalence and costs of skin cancer treatment in the U.S., 2002–2006 and 2007–2011. *Am. J. Prev. Med.* **48**, 183-187. doi:10.1016/j.amepre.2014.08.036
Hahn, W. C., Counter, C. M., Lundberg, A. S., Beijersbergen, R. L., Brooks, M. W. and Weinberg, R. A. (1999). Creation of human tumour cells with defined genetic elements. *Nature* **400**, 464-468. doi:10.1038/22780
Hart, K. C., Tan, J., Siemers, K. A., Sim, J. Y., Pruitt, B. L., Nelson, W. J. and Gloerich, M. (2017). E-cadherin and LGN align epithelial cell divisions with tissue tension independently of cell shape. *Proc. Natl. Acad. Sci. USA* **114**, E5845-E5853. doi:10.1073/pnas.1701703114
Hinck, L. and Näthke, I. (2014). Changes in cell and tissue organization in cancer of the breast and colon. *Curr. Opin. Cell Biol.* **26**, 87-95. doi:10.1016/j.ceb.2013.11.003
Hussein, M. R. (2005). Ultraviolet radiation and skin cancer: molecular mechanisms. *J. Cutan. Pathol.* **32**, 191-205. doi:10.1111/j.0303-6987.2005.00281.x
Iden, S., van Riel, W. E., Schäfer, R., Song, J.-Y., Hirose, T., Ohno, S. and Collard, J. G. (2012). Tumor type-dependent function of the par3 polarity protein in skin tumorigenesis. *Cancer Cell* **22**, 389-403. doi:10.1016/j.ccr.2012.08.004
Katzenellenbogen, B. S., Norman, M. J., Eckert, R. L., Peltz, S. W. and Mangel, W. F. (1984). Bioactivities, estrogen receptor interactions, and plasminogen activator-inducing activities of tamoxifen and hydroxy-tamoxifen isomers in MCF-7 human breast cancer cells. *Cancer Res.* **44**, 112-119.
Khavari, P. A. (2006). Modelling cancer in human skin tissue. *Nat. Rev. Cancer* **6**, 270-280. doi:10.1038/nrc1838
LaMonica, B. E., Lui, J. H., Hansen, D. V. and Kriegstein, A. R. (2013). Mitotic spindle orientation predicts outer radial glial cell generation in human neocortex. *Nat. Commun.* **4**, 1665. doi:10.1038/ncomms2647
Lazarov, M., Kubo, Y., Cai, T., Dajee, M., Tarutani, M., Lin, Q., Fang, M., Tao, S., Green, C. L. and Khavari, P. A. (2002). CDK4 coexpression with Ras generates malignant human epidermal tumorigenesis. *Nat. Med.* **8**, 1105-1114. doi:10.1038/nm779
Lechler, T. and Fuchs, E. (2005). Asymmetric cell divisions promote stratification and differentiation of mammalian skin. *Nature* **437**, 275-280. doi:10.1038/nature03922
Li, J. and Sen, G. L. (2015). Generation of genetically modified organotypic skin cultures using devitalized human dermis. *J. Vis. Exp.* **106**, e53280. doi:10.3791/53280
Li, M., Sun, Q. and Wang, X. (2017). Transcriptional landscape of human cancers. *Oncotarget* **8**, 34534-34551. doi:10.18632/oncotarget.15837
Li, J., Chen, Y., Xu, X., Jones, J., Tiwari, M., Ling, J., Wang, Y., Harismendy, O. and Sen, G. L. (2019). HNRNPK maintains epidermal progenitor function through transcription of proliferation genes and degrading differentiation promoting mRNAs. *Nat. Commun.* **10**, 4198. doi:10.1038/s41467-019-12238-x
Lough, K. J., Byrd, K. M., Descovich, C. P., Spitzer, D. C., Bergman, A. J., Beaudoin, G. M. J., III, Reichardt, L. F. and Williams, S. E. (2019). Telophase correction refines division orientation in stratified epithelia. *eLife* **8**, e49249. doi:10.7554/eLife.49249
McCaffrey, L. M. and Macara, I. G. (2011). Epithelial organization, cell polarity and tumorigenesis. *Trends Cell Biol.* **21**, 727-735. doi:10.1016/j.tcb.2011.06.005
McCaffrey, L. M., Montalbano, J. A., Mihai, C. and Macara, I. G. (2016). Loss of the Par3 polarity protein promotes breast tumorigenesis and metastasis. *Cancer Cell* **30**, 351-352. doi:10.1016/j.ccell.2016.07.001
Mescher, M., Jeong, P., Knapp, S. K., Rübsam, M., Saynisch, M., Kranen, M., Landsberg, J., Schlaak, M., Mauch, C., Tüting, T. et al. (2017). The epidermal polarity protein Par3 is a non-cell autonomous suppressor of malignant melanoma. *J. Exp. Med.* **214**, 339-358. doi:10.1084/jem.20160596
Mistry, D. S., Chen, Y. and Sen, G. L. (2012). Progenitor function in self-renewing human epidermis is maintained by the exosome. *Cell Stem Cell* **11**, 127-135. doi:10.1016/j.stem.2012.04.022
Miyashita, S., Adachi, T., Yamashita, M., Sota, T. and Hoshino, M. (2017). Dynamics of the cell division orientation of granule cell precursors during cerebellar development. *Mech. Dev.* **147**, 1-7. doi:10.1016/j.mod.2017.06.002
Neumüller, R. A. and Knoblich, J. A. (2009). Dividing cellular asymmetry: asymmetric cell division and its implications for stem cells and cancer. *Genes Dev.* **23**, 2675-2699. doi:10.1101/gad.1850809
Pickering, C. R., Zhou, J. H., Lee, J. J., Drummond, J. A., Peng, S. A., Saade, R. E., Tsai, K. Y., Curry, J. L., Tetzlaff, M. T., Lai, S. Y. et al. (2014). Mutational landscape of aggressive cutaneous squamous cell carcinoma. *Clin. Cancer Res.* **20**, 6582-6592. doi:10.1158/1078-0432.CCR-14-1768
Poulson, N. D. and Lechler, T. (2010). Robust control of mitotic spindle orientation in the developing epidermis. *J. Cell Biol.* **191**, 915-922. doi:10.1083/jcb.201008001
Rangarajan, A., Hong, S. J., Gifford, A. and Weinberg, R. A. (2004). Species- and cell type-specific requirements for cellular transformation. *Cancer Cell* **6**, 171-183. doi:10.1016/j.ccr.2004.07.009
Repasky, G. A., Chenette, E. J. and Der, C. J. (2004). Renewing the conspiracy theory debate: does Raf function alone to mediate Ras oncogenesis? *Trends Cell Biol.* **14**, 639-647. doi:10.1016/j.tcb.2004.09.014
Reuter, J. A., Ortiz-Urda, S., Kretz, M., Garcia, J., Scholl, F. A., Pasmooij, A. M. G., Cassarino, D., Chang, H. Y. and Khavari, P. A. (2009). Modeling inducible human tissue neoplasia identifies an extracellular matrix interaction

network involved in cancer progression. *Cancer Cell* **15**, 477-488. doi:10.1016/j.ccr.2009.04.002

Ridky, T. W., Chow, J. M., Wong, D. J. and Khavari, P. A. (2010). Invasive three-dimensional organotypic neoplasia from multiple normal human epithelia. *Nat. Med.* **16**, 1450-1455. doi:10.1038/nm.2265

Robertson, D. W., Katzenellenbogen, J. A., Long, D. J., Rorke, E. A. and Katzenellenbogen, B. S. (1982). Tamoxifen antiestrogens. A comparison of the activity, pharmacokinetics, and metabolic activation of the cis and trans isomers of tamoxifen. *J. Steroid Biochem.* **16**, 1-13. doi:10.1016/0022-4731(82)90137-6

Rogers, H. W., Weinstock, M. A., Feldman, S. R. and Coldiron, B. M. (2015). Incidence estimate of nonmelanoma skin cancer (Keratinocyte Carcinomas) in the U.S. population, 2012. *JAMA Dermatol.* **151**, 1081-1086. doi:10.1001/jamadermatol.2015.1187

Scholl, F. A., Dumesic, P. A., Barragan, D. I., Harada, K., Bissonauth, V., Charron, J. and Khavari, P. A. (2007). Mek1/2 MAPK kinases are essential for Mammalian development, homeostasis, and Raf-induced hyperplasia. *Dev. Cell* **12**, 615-629. doi:10.1016/j.devcel.2007.03.009

Scholl, F. A., Dumesic, P. A., Barragan, D. I., Harada, K., Charron, J. and Khavari, P. A. (2009). Selective role for Mek1 but not Mek2 in the induction of epidermal neoplasia. *Cancer Res.* **69**, 3772-3778. doi:10.1158/0008-5472.CAN-08-1963

Sen, G., Wehrman, T. S., Myers, J. W. and Blau, H. M. (2004). Restriction enzyme-generated siRNA (REGS) vectors and libraries. *Nat. Genet.* **36**, 183-189. doi:10.1038/ng1288

Sen, G. L., Reuter, J. A., Webster, D. E., Zhu, L. and Khavari, P. A. (2010). DNMT1 maintains progenitor function in self-renewing somatic tissue. *Nature* **463**, 563-567. doi:10.1038/nature08683

Stemmler, M. P., Eccles, R. L., Brabletz, S. and Brabletz, T. (2019). Non-redundant functions of EMT transcription factors. *Nat. Cell Biol.* **21**, 102-112. doi:10.1038/s41556-018-0196-y

Suzuki, A. and Ohno, S. (2006). The PAR-aPKC system: lessons in polarity. *J. Cell Sci.* **119**, 979-987. doi:10.1242/jcs.02898

Tadeu, A. M. B. and Horsley, V. (2014). Epithelial stem cells in adult skin. *Curr. Top. Dev. Biol.* **107**, 109-131. doi:10.1016/B978-0-12-416022-4.00004-4

Vorhagen, S., Kleefisch, D., Persa, O.-D., Graband, A., Schwickert, A., Saynisch, M., Leitges, M., Niessen, C. M. and Iden, S. (2018). Shared and independent functions of aPKCλ and Par3 in skin tumorigenesis. *Oncogene* **37**, 5136-5146. doi:10.1038/s41388-018-0313-1

Wang, Y., Arribas-Layton, M., Chen, Y., Lykke-Andersen, J. and Sen, G. L. (2015). DDX6 orchestrates mammalian progenitor function through the mRNA degradation and translation pathways. *Mol. Cell* **60**, 118-130. doi:10.1016/j.molcel.2015.08.014

Wang, X., Dong, B., Zhang, K., Ji, Z., Cheng, C., Zhao, H., Sheng, Y., Li, X., Fan, L., Xue, W. et al. (2018). E-cadherin bridges cell polarity and spindle orientation to ensure prostate epithelial integrity and prevent carcinogenesis in vivo. *PLoS Genet.* **14**, e1007609. doi:10.1371/journal.pgen.1007609

Williams, S. E. and Fuchs, E. (2013). Oriented divisions, fate decisions. *Curr. Opin. Cell Biol.* **25**, 749-758. doi:10.1016/j.ceb.2013.08.003

Williams, S. E., Beronja, S., Pasolli, H. A. and Fuchs, E. (2011). Asymmetric cell divisions promote Notch-dependent epidermal differentiation. *Nature* **470**, 353-358. doi:10.1038/nature09793

Williams, S. E., Ratliff, L. A., Postiglione, M. P., Knoblich, J. A. and Fuchs, E. (2014). Par3-mInsc and Gαi3 cooperate to promote oriented epidermal cell divisions through LGN. *Nat. Cell Biol.* **16**, 758-769. doi:10.1038/ncb3001

Xue, B., Krishnamurthy, K., Allred, D. C. and Muthuswamy, S. K. (2013). Loss of Par3 promotes breast cancer metastasis by compromising cell-cell cohesion. *Nat. Cell Biol.* **15**, 189-200. doi:10.1038/ncb2663

Zen, K., Yasui, K., Gen, Y., Dohi, O., Wakabayashi, N., Mitsufuji, S., Itoh, Y., Zen, Y., Nakanuma, Y., Taniwaki, M. et al. (2009). Defective expression of polarity protein PAR-3 gene (PARD3) in esophageal squamous cell carcinoma. *Oncogene* **28**, 2910-2918. doi:10.1038/onc.2009.148

Zeng, G., Taylor, S. M., McColm, J. R., Kappas, N. C., Kearney, J. B., Williams, L. H., Hartnett, M. E. and Bautch, V. L. (2007). Orientation of endothelial cell division is regulated by VEGF signaling during blood vessel formation. *Blood* **109**, 1345-1352. doi:10.1182/blood-2006-07-037952

Zhang, X., Liu, L., Deng, X., Li, D., Cai, H., Ma, Y., Jia, C., Wu, B., Fan, Y. and Lv, Z. (2019). MicroRNA 483-3p targets Pard3 to potentiate TGF-β1-induced cell migration, invasion, and epithelial-mesenchymal transition in anaplastic thyroid cancer cells. *Oncogene* **38**, 699-715. doi:10.1038/s41388-018-0447-1

Žigman, M., Cayouette, M., Charalambous, C., Schleiffer, A., Hoeller, O., Dunican, D., McCudden, C. R., Firnberg, N., Barres, B. A., Siderovski, D. P. et al. (2005). Mammalian inscuteable regulates spindle orientation and cell fate in the developing retina. *Neuron* **48**, 539-545. doi:10.1016/j.neuron.2005.09.030

Figure S1

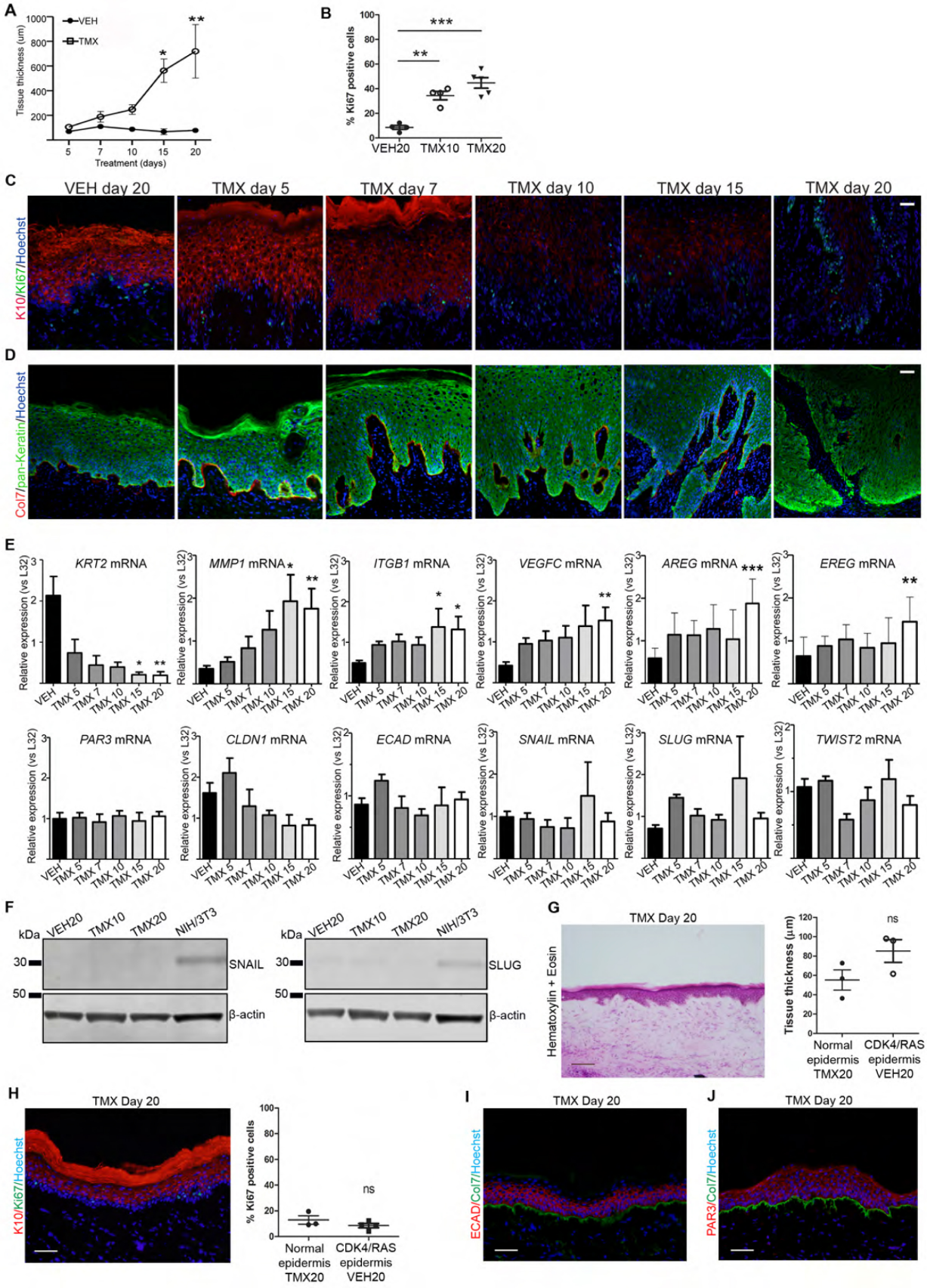

Figure S1. Changes associated with early human tumorigenesis. Related to Figure 1.

(A) Epidermal hyperplasia in CDK4/RAS xenografts after 20 days treatment with TMX or VEH. n= 3-6 xenografted mice measured per timepoint. *p<0.05, **p<0.01 relative to VEH treated mice. Statistical significance was calculated using two-way ANOVA. **(B)** Quantification of Ki67 positive cells for images shown in **(C).** n=4-5 mice were measured per group. **p<0.01, ***p<0.001 relative to VEH20. Statistical significance was calculated using one-way ANOVA. **(C)** CDK4/RAS regenerated epidermis, at indicated timepoints of TMX/VEH, is co-labeled with proliferation marker, Ki67 (green), differentiation marker, K10 (red), and nuclear stain Hoechst (blue). **(D)** CDK4/RAS grafts were immunostained with pan keratin (green) and collagen VII (Col7: red). Scale bar=20μm, n=3-6 xenografted animals analyzed per timepoint. **(E)** mRNA expression of oncogenic, differentiation, cell adhesion and polarity markers during tumor progression. n=4-16 xenografts were analyzed per timepoint, per group. Statistical significance was calculated using one-way ANOVA. **(F)** Western blot and densitometry of SNAIL and SLUG protein in CDK4/RAS xenografts treated with VEH or TMX at indicated timepoints. NIH/3T3 cell lysate was used as positive control. β was u was used as loading control. Blot representative of n=3 animals per timepoint **(G)** H&E staining and epidermis thickness of normal keratinocyte xenografts treated with TMX for 20 days. Scale bar=50μm, n=3 animals were analyzed. Right panel: quantitation of epidermal thickness. ns = not significant. Statistical significance was calculated using unpaired t-test. **(H)** Ki67 and K10 immunostaining of normal keratinocyte xenografts treated with TMX for 20 days. Scale bar=20μm**.** Right panel: quantification of Ki67 positive cells. n=3 animals were analyzed. ns = not significant. Statistical significance was calculated using unpaired t-test. **(I)** Representative images of ECAD (red) and Collagen VII (Col7: green) immunostaining and **(J)** PAR3 (red) and Col7 (green) immunostaining. Scale bar=20μm. All data represented as mean±SEM.

Figure S2

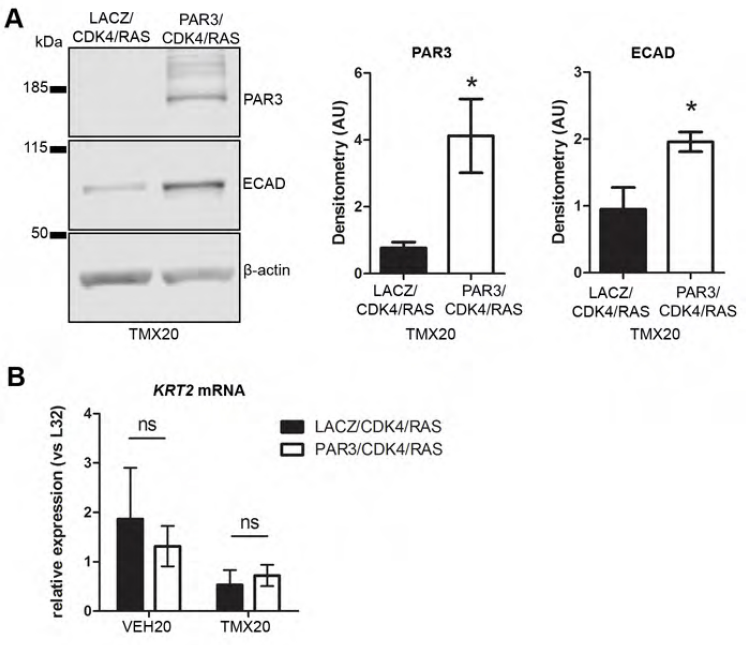

Figure S2.

(A) ECAD and PAR3 protein expression after 20 days of TMX treatment by Western blotting. Densitometry based on n=3 mice per group. Statistical significance was calculated by unpaired t-test. *p<0.05 relative to VEH. **(B)** mRNA expression of epidermis differentiation marker Keratin 2 (KRT2) after VEH and TMX treatment. n=3-6 mice were analyzed per group. Statistical significance was calculated using two-way ANOVA. ns=not significant. All data represented as mean±SEM.

Figure S3.

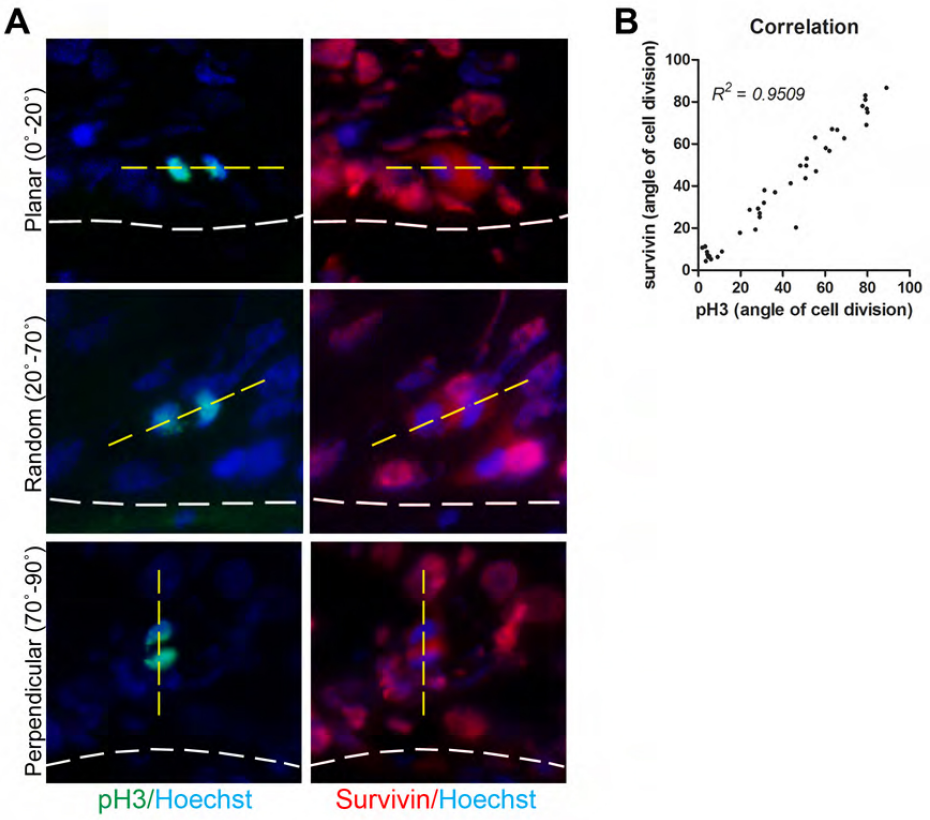

Figure S3. Correlation of cell division angles between pH3 and Survivin. Related to Figure 3.

(A) Representative orientation of cell divison in cells immunostained with pH3 (green) and Survivin (red). Planar (0°-20°), random (20°-70°), and perpendicular (70°-90°) divisions are defined relative to the basement membrane (denoted by the dotted white line). **(B)** R_2 linear regression analysis comparing Survivin determined division angles with pH3 determined cell division angles. Each dot represents a cell division angle determined by survivin and pH3 staining.